Sensitivity Modulated Inversion for the Post-seismic Deformation of the Great 11 March 2011 Tohoku-Oki (Mw 9.0) Earthquake

Francisco Ortega[1] (ortega@gps.caltech.edu), Mark Simons[1], Susan Owen[2], Angelyn Moore[2], Rowena Lohman[3]

(1) Seismological Laboratory, California Institute of Technology, Pasadena, California 91125, USA. (2) Jet Propulsion Laboratory, Pasadena, CA 91109, USA. (3) Department of Earth and Atmospheric Sciences, Cornell University, Ithaca, NY 14853, United States.

Abstract

We infer the spatial distribution of after-slip following the Mw 9.0 11 March 2011 Tohoku-Oki, Japan earthquake and discuss the implications of this after-slip in the context of a future large earthquake in the Ibaraki region which lies to the south of the March 11, 2011 event. Our after-slip models are constrained by onshore GPS time series. To infer the distribution of slip, we adopt a non-negative least squares approach, with a novel regularization that imposes a stronger correlation among neighboring patches in the regions of the megathrust with lower sensitivity, thereby improving the stability of the model. Relative to conventional approaches that assume a spatially constant regularization, this approach permits us to infer more detail in the distribution of slip where the model is well constrained while at the same time limiting the number of artifacts introduced in the less constrained portion of the model. Our results indicate that after-slip occurs mainly downdip and south of the region that experienced large co-seismic slip during the Mw 9.0 event and also at a the Sanriku-Oki low seismicity region, believed to undergo aseismic creep close to plate convergence rate. Also, the shallower part of the megathrust at the Ibaraki region has, on average, around 1+ meters of slip during the first 6 months after the Tohoku-Oki mainshock. Although our analysis may indicate that the upper part of the megathrust at the Ibaraki region is undergoing post-seismic slip, further study is required to accurately assess the risk of a great Earthquake at the southern portion of the Japan megathrust. The complexity of the inferred after slip and its relationship to the distribution of co-seismic fault slip and seismicity, along with the geodetically inferred coupling models, suggests strong heterogeneity in of in the spatial distribution of material properties on the megathrust.

The Tohoku-oki Earthquake

Figure 1:

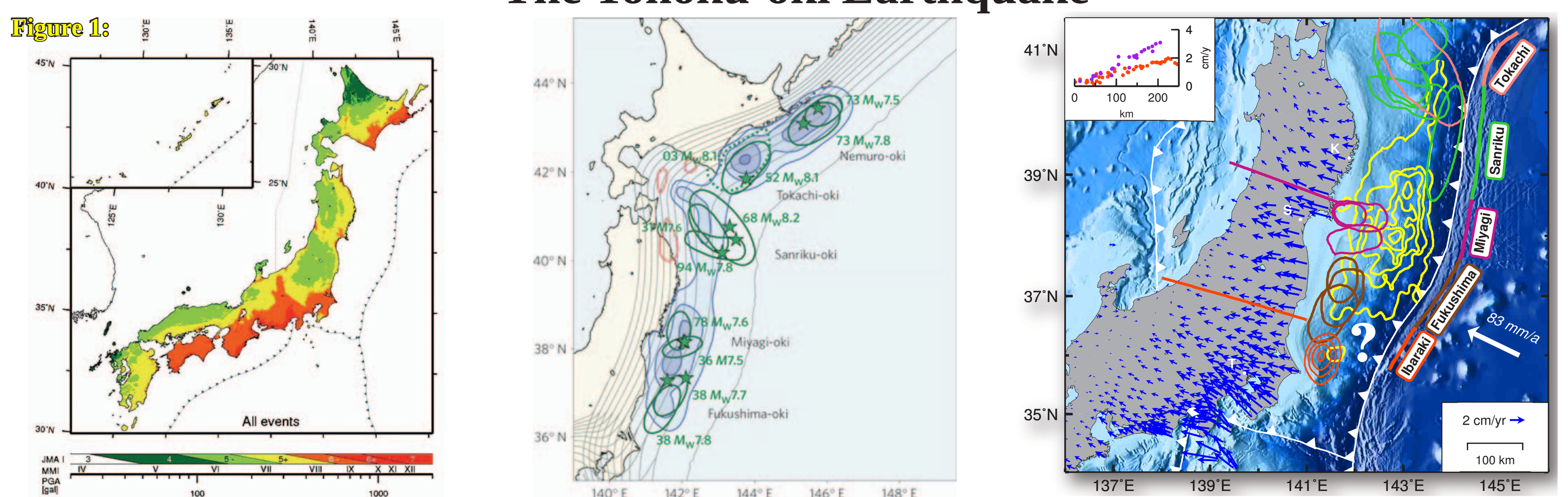

(a) Probabilistic Seismic Hazard Map of Japan Maximum predicted intensity in 500 yrs. Miyazawa and Mori [2009], BSSA.

(b) Interplate seismogenic "stuck" zones along the Kuril-Japan trench inferred from GPS data inversion. Hashimoto et al [2009], Nature Geoscience.

(a) Co-seismic model of the 2011 Tohoku-oki (Mw9.0) earthquake (yellow 10m slip contours). Historical earthquakes (ellipses). Interseismic velocity field (blue arrows). Suggest potential for a large earthquake off-shore Ibaraki. Simons et al. [2011], Science.

Before the Tohoku-oki earthquake the Tohoku region of the Japan Trench megathrust was considered to have a moderate seismic hazard and many inter-seismic coupling models suggested that regions of significant fault coupling were broadly limited to regions that had experienced earthquakes over the last centuries - with either negligible or limited coupling in much of the region that slipped co-seismically during 2011. Thus, the Tohoku-oki earthquake underscored our need to improve our understanding and assessment of the spatial variability in the slip budget integrated throughout the seismic cycle at subduction megathrust, essential for both the understanding of the rheological nature of the megathrust as well as for seismic hazard assessment. We are particularly concerned with the region off-shore Ibaraki, just south of the rupture area of the Tohoku-oki earthquake, where the potential for a large earthquake is still unclear.

Continuous GPS Data Processing

Raw data from cGPS sites is processed using the software GIPSY (Japan) to produce positional time series for each site on the GPS network. The positional time series contain a secular motion due to interseismic tectonic loading, earthquake associated signals (co- and post- seismic), a seasonal term associated with weather related crustal loading and gravity, as well as anthropogenic signals such as changes in hardware, or location of each site.

We identify and separate the different signals in the positional time series by an iterative process in which a motion coherent to the whole continuous GPS network is also estimated and removed, allowing a precise estimation of the features present in the time series.

Figure 2:

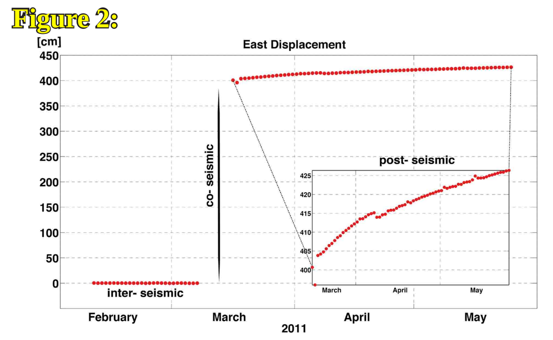

(a) Example of positional (daily) time series from continuous GPS in Japan. Signals from the 3 stages of the seismic cycle are labeled, where the co-seismic jump corresponds to the one of the 11 March 2011, Tohoku-Oki earthquake. The inset shows the post-seismic motion induced by such event as well as signals from several aftershocks.

$$u(t) = u_0 + v \cdot t + \sum_i \left[EQco_i(t) + EQpos_i(t)\right] + \sum_k \left[\beta^k H(t-t^k)\right] + S(t)$$

where

$$EQco_i(t) = u_c^i H(t-t_0^i)$$
$$EQpos_i(t) = \alpha_R^i log\left(1 + \frac{(t-t_0^i)}{\tau} H(t-t_0^i)\right)$$
$$HW_i(t) = \beta^k H(t-t^k)$$
$$S(t) = \left\langle sin\left(\frac{t}{T_1}+\phi_1\right), sin\left(\frac{t}{T_2}+\phi_2\right)\right\rangle$$

(b) Model used to separate the signals present in the positional time series. A weighted least squares fit is performed to obtain the contribution of each signal in the positional data. Note that the earthquake and hardware changes times are assumed to be known, so inspection of all time series is required.

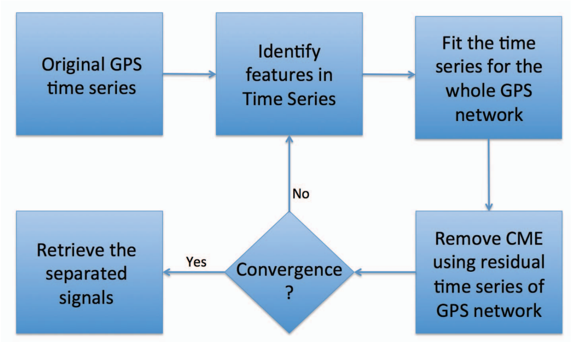

(c) Diagram describing the iterative process used to identify and separate the different features present in the positional time series.

Figure 3:

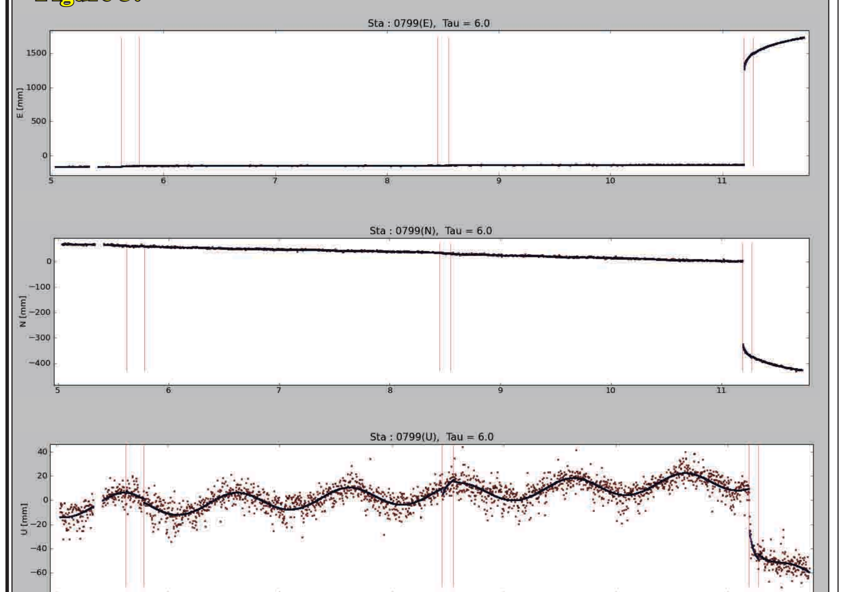

Example of positional (daily) time series for a continuous GPS site from the GEONET network in Japan (site 0799). Note the magnitude is the seasonal signal in the vertical position of site 0799. We use the GEONET time series to estimate the co- and post- seismic displacements associated to the Tohoku-Oki earthquake.

Figure 4: **Data used in this study**

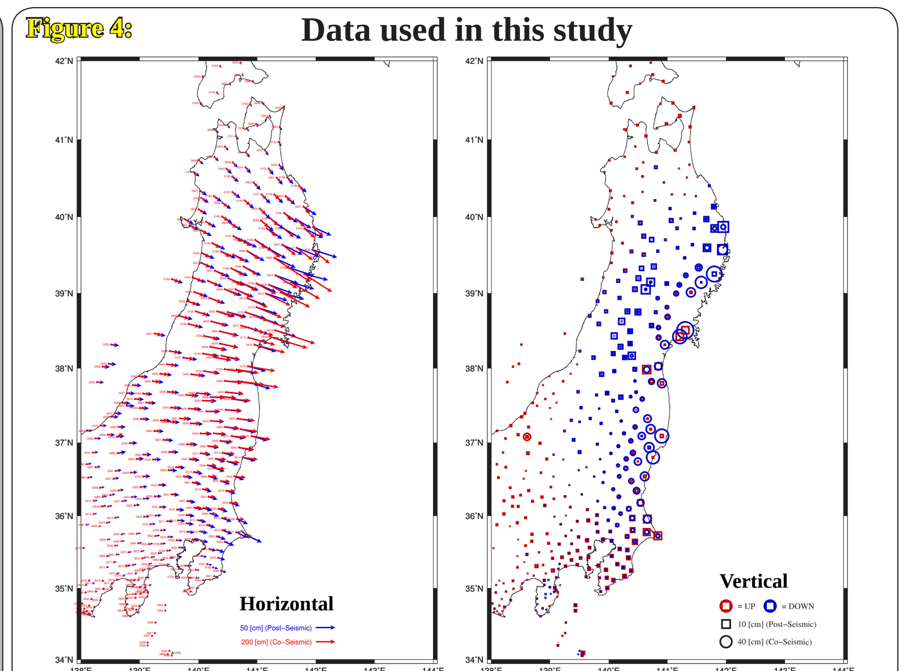

Co- and Post- seismic displacements associated to the 11 March 2011 (M9.0) Tohoku-Oki earthquake. Post-seismic displacements are estimated up to Sep 01, 2011. Note the change in direction of the horizontal post-seismic displacement with respect the co-seismic in northern Honshu, as well as the hinge line change from off-shore for the mainshock to inland for the post-seismic displacements.

Least Squares Slip Inversion and Variable Regularization Approach

To solve for the after slip of the Tohoku-Oki earthquake we perform a damped Least Squares inversion with weights defined as the inverse of the misfit variances. We constrain the dip slip component of the after slip to be non negative. We minimize the functional:

$$\psi(m) = \|W_d(Gm-d)\|_2^2 + \lambda^2 \|W_R T m\|_2^2$$

Where W_d is the misfit weights matrix (inverse of covariance), G is the design matrix of the problem, m is the after slip, λ is a parameter to define the strength of the regularization, and d is the vector of observations at the GPS sites. The form of regularization adopted is to minimize a weighted Laplacian operator (T) applied to the fault slip distribution. W_R allows for a variable strength of the smoothing operator T, defined as a function of the sensitivity of the fault patches.

The sensitivity of the fault patches (S_R, Figure 5) is defined as the squared surface displacements, integrated throughout the GPS network, due to an unit dislocation at the fault patch. We propose that the sensitivity can be interpreted as a measure of fault patch slip "resolution" as it indicates its capacity to contribute to the fault slip model predicted displacements at the GPS network. Note the high variability of S_R, 100 m of slip near the trench is equivalent to 1 m of slip at the coastline.

To account for the variability in sensitivity during the inversion, we modulate strength of the Laplacian operator in function of the sensitivity of the patch. We define such a strengthening factors W_R as the square root of the reciprocal of the patch's sensitivity. Then,

$$W_R = \sqrt{S_R^{-1}} \qquad S_R = \frac{1}{c} diag(G^t G) \qquad c = \mathrm{MAX}(diag(G^t G))$$

The net impact of the modulated smoothing is to adjust the correlation length of the slip at the patches according to the strength of the constraints provided by the observables. Thus allowing more complex (rougher) slip distributions at the well constrained regions of the megathrust while imposing smoother slip distributions at the least constrained ones.

Figure 5:

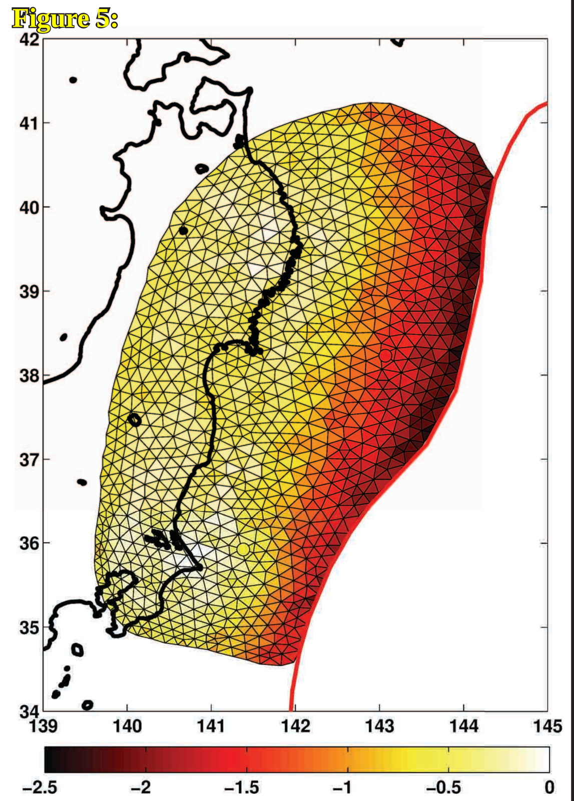

Fault patch Relative Sensitivity (Log-scale). Adapted from Loveless and Meade [2011] to be consistent with L2 norm for least squares inversion. Note how the sensitivity decreases with its distance from the on-shore GPS network.

We use a 3D triangulated surface obtained from regional seismicity and seismic profiles to model the Japan trench megathrust (Ye et al [2012], Simons et al[2011] and references thereinto). The media is represented by 1D layered elastic structure with properties computed by averaging 3D tomography at the Tohoku-oki rupture area (3D tomography from NIED and Takahashi et al. [2004]).

Checkerboard Test

To show the importance of using the sensitivity modulated Laplacian operator to smooth the afterslip, we perform 2 checkerboard tests, with an uniform (constant) Laplacian operator and with the sensitivity modulated Laplacian operator defined in this work. We use 2 synthetic datasets that differ only in the realization of the random noise. Note how the sensitivity regularization able us to recover a much more stable slip distribution, an overall rougher model while imposing stronger smoothing at the regions with lower sensitivity and to consistently achieve a better recovery of the target slip distribution. The main advantage of the proposed regularization is that we are able to make an interpretation of the obtained slip distribution at the regions with low sensitivity as a low resolution average of the true slip. The value recovered is close to the spatial average of the target slip.

Figure 6:

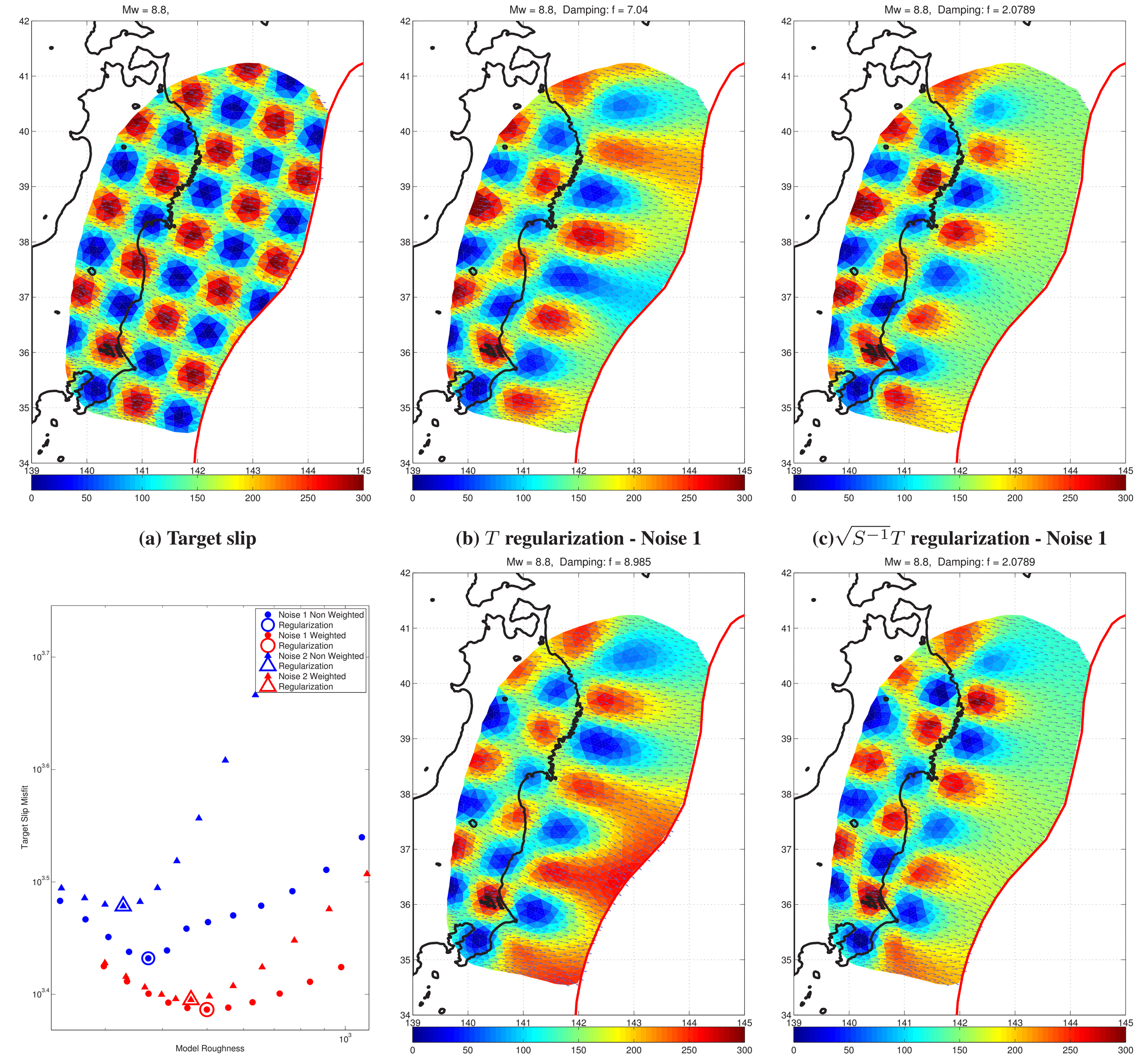

(a) Target slip

(b) T regularization - Noise 1

(c) $\sqrt{S^{-1}}T$ regularization - Noise 1

(d) Target Slip Misfit v/s Slip Roughness

(e) T regularization - Noise 2

(f) $\sqrt{S^{-1}}T$ regularization - Noise 2

(a) Input checkerboard after-slip model used to generate synthetic displacements at the GPS site locations. Two sets of synthetic observations are generated by independent realizations of a Gaussian noise, Noise 1 and Noise 2, based on observational variances. We perform slip inversion tests constrained by the synthetic observations using the uniform Laplacian regularization of the slip distribution (b and e) and using the sensitivity modulated regularization proposed in this study (c and f). (b) and (c) uses the synthetic data with added Noise1, (e) and (f) use Noise2. When using the proposed regularization approach, the recovered after-slip at the regions of low sensitivity is approximately the average of the target model. On the contrary, the results obtained using the uniform Laplacian shows poorly resolved and unstable after-slip distribution, obtaining values smeared from the regions of high sensitivity. (d) Target slip RMS residual v/s slip roughness for the inversions using both regularization schemes. Open symbols indicate the optimum solutions. Note how the sensitivity regularization able us to recover solutions with a smaller misfit and an overall rougher slip distribution while imposing a stronger smoothing at the least sensitive regions of the fault surface. For comparison purposes, the roughness is computed as $\|T \cdot m\|_2$ for both regularization cases.

Results and Discussion

We use the geodetic data shown in Figure 4 to invert for post-seismic slip models associated to the 2011 Tohoku-oki (Mw9.0) earthquake. Here we show an after-slip model that was selected as a representative model of the solution space of the inverse problem. A criteria of compatibility with independent geophysical observations in conjunction with the L-curve criteria were used to select the strength of the regularization (damping parameter). After-slip occurs mostly downdip and south of the rupture region of the Tohoku-oki main shock. Note the compacity and rich spatial variation of the inferred after-slip.

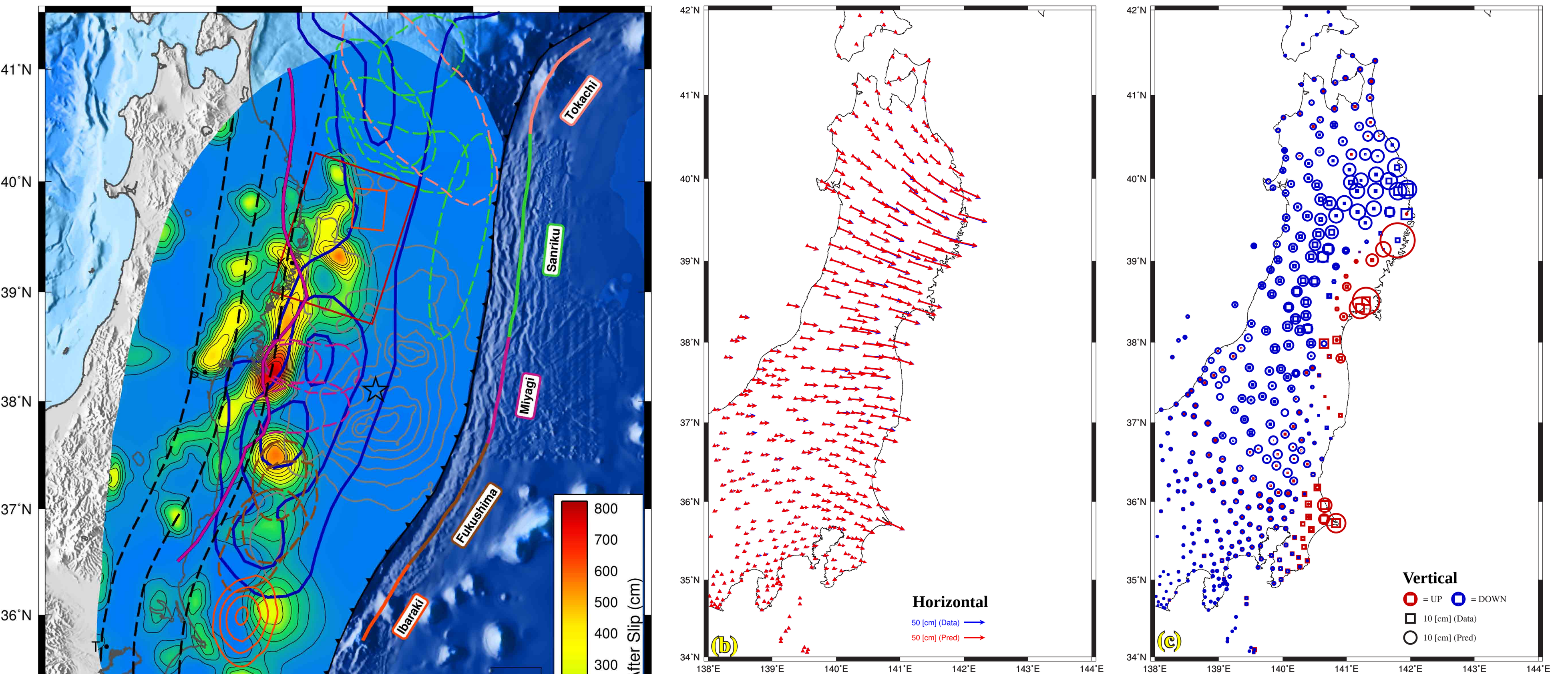

Figure 7: (a) Inferred after-slip from 6 months of GPS observations. Gray contours (8m) : co-seismic slip for Tohoku-Oki mainshock, orange contours (1m) : co-seismic slip for M7.9 aftershock, from Simons et al. [2011]. Blue contours: coupling model from Hashimoto et al. [2009]. Dashed black lines : 50, 70, 90 km depth plate interface contours. Solid red line: downdip limit of seismicity (Igarashi et al. [2001]). Closed dashed lines delineate historical events colored by region. Red rectangle indicates the Sanriku-oki low seismicity region (Ye et al. [2012]). Star indicates JMA centroid for Tohoku-oki. (b) and (c): comparison of observed and predicted post-seismic displacements at GPS network.

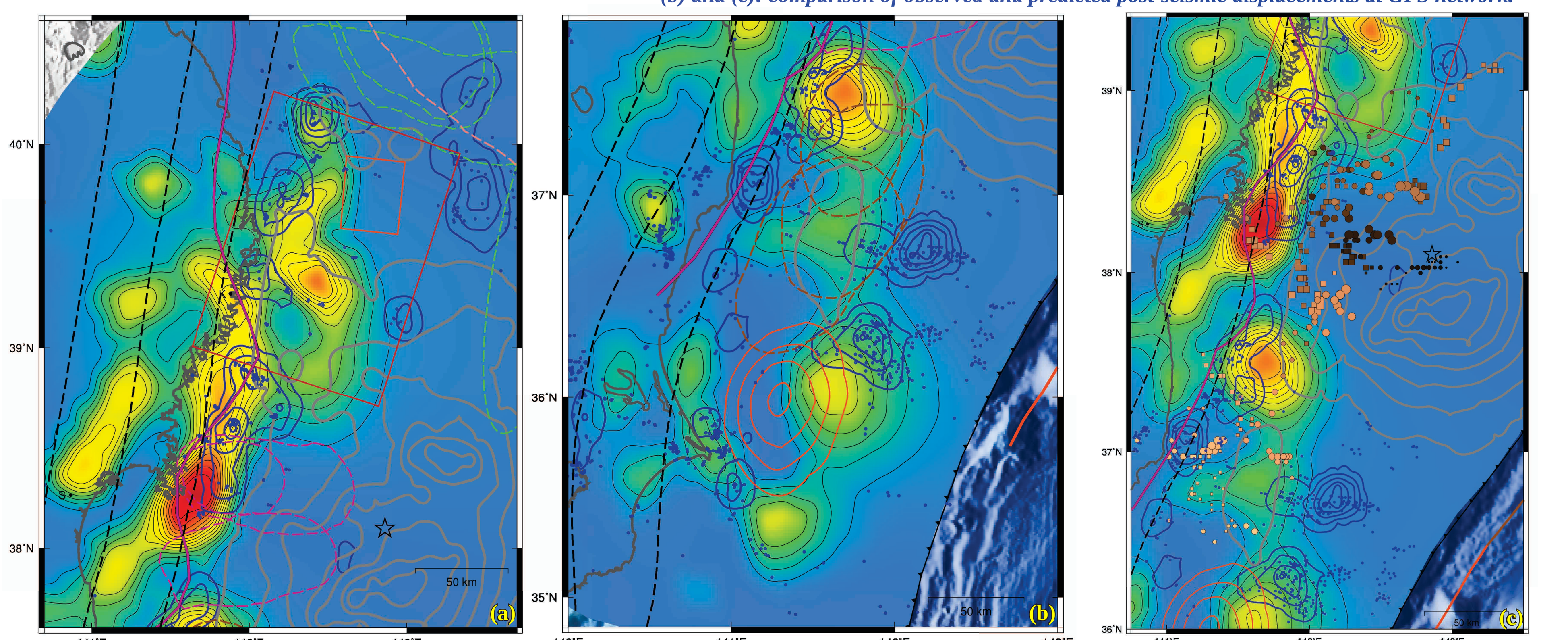

Figure 8: (a) Zoom in northern Tohoku. Blue contours and dots indicate thrust aftershock density and repeaters from Kato et al. [2012]. Note how aftershocks distribute in compact regions and how these tend to localize at the edges of the regions of post-seismic slip. Also note how co- and post- seismic slip coincide at the Sanriku-oki low seismicity region. Such region was suggested to be in a rate strengthening frictional regime. Orange box indicate Mw7.4 aftershock.

(b) Zoom in southern Tohoku. Features same as in (a). Post-seismic slip occurs mostly at the updip part of the megathrust off-shore Ibaraki and surrounding the Mw7.9 aftershock (orange contours). After-slip occurred updip in the megathrust, during the first 6 months after the mainshock, is equivalent to a Mw8.0 earthquake. The location of the repeater aftershocks suggests that after-slip is occurring up to trench depths.

(c) Brown colored dots indicate the location of high frequency radiators associated to the Tohoku-oki mainshock (Simons et al. [2011]). Note how the HF radiators tend to locate between the regions of co- and post-seismic slip and surrounding the highest peaks of after-slip, reinforcing the hypothesis that these indicate the location of brittle asperities embedded in a ductile matrix (Simons et al. [2011]).

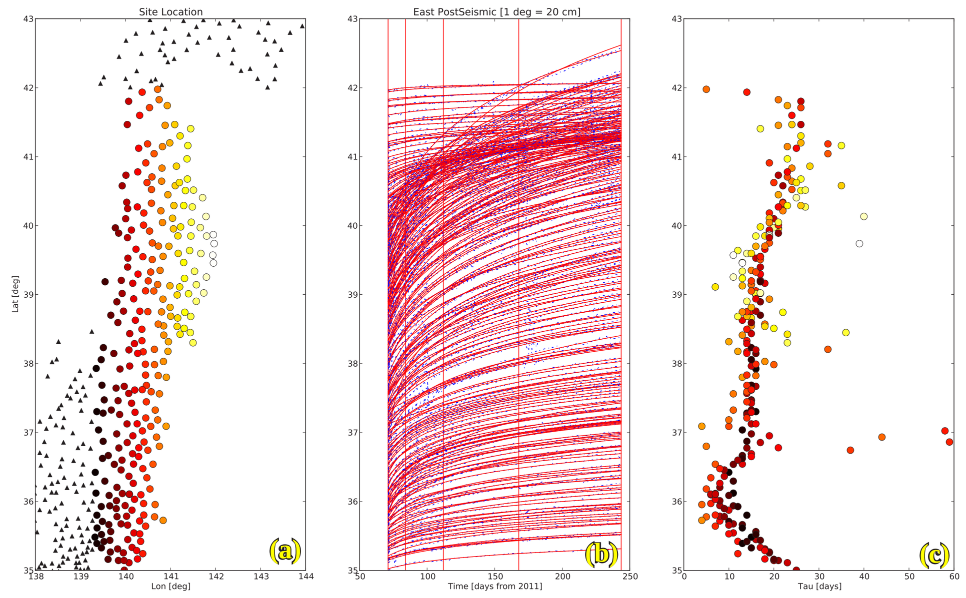

Figure 9: Estimation of the characteristic time of the post-seismic transient modeled as a log-decay function. (a) Circles colored by longitude in left panel indicate the sites whose post-seismic time series were modeled using a logarithmic decay function. (b) GPS time series (blue dots) and fitted models (red lines) in which the characteristic time is obtained by a grid search process. (c) Estimated characteristic time for the selected GPS sites. Note how these are clustered and define curve as a function of the latitude. The coherent variations in the characteristic time suggest a latitudinal variability in the rheological parameters of the Japan trench megathrust.

We develop a spatially variable regularization based on fault sensitivity that presents a real improvement for the least squares slip inversion problem over previous uniform regularization schemes.

Overall we observe extremely heterogeneous characteristics of the distributions of slip behavior during the seismic cycle at the Japan megathrust. Together, the complexity of thrust aftershock, afterslip distribution, source region of the Tohoku-Oki earthquake and variations in characteristic relaxation time of post-seismic GPS time series, suggests a strong heterogeneity in the spatial distribution of material properties on the Japan megathrust.

The potential for a large earthquake off-shore Ibaraki remains unclear. The geodetic inferred long term slip rate accumulation at the Japan trench is considerably larger than the one released by historical earthquakes and the inferred after-slip only accounts for a fraction of the slip budget off-shore Ibaraki. Possible mechanisms to balance the slip budget may include the occurrence of Tohoku-oki type earthquakes, episodes of aseismic slip, or creep at rates close to plate convergence. The limitations of the inverse problem posed by the spatial distribution of the available geodetic measurements (on-shore) makes impossible to discriminate which mechanisms are responsible for balancing the slip budget off-shore Ibaraki.

We need to implement a continuous monitoring of the underwater portion of the megathrust in order to accurately assess its behavior.